

PERFORMANCE EVALUATION OF 16APSK AND SOQPSK-TG IN THE PRESENCE OF POLARIZATION COMBINING IN AERONAUTICAL TELEMETRY

Farah Arabian, Michael Rice

Department of Electrical and Computer Engineering

Brigham Young University

Provo, UT, 84602

farah.arabian@byu.edu, mdr@byu.edu

ABSTRACT

16-ary amplitude phase shift keying (16APSK) is a candidate modulation for aeronautical mobile telemetry because it has better spectral efficiency and lower sensitivity to adjacent channel interference compared SOQPSK-TG. This paper compares the post-equalizer bit error rate performance of 16APSK and SOQPSK-TG in the aeronautical mobile telemetry multipath channel. The linear polarizations produced by the orthogonal dipoles in the receive antenna feed are combined in two different ways: using a 90° hybrid coupler to produce RHCP or LHCP and maximum likelihood combining. The first combining method is the common practice at test ranges and the second combining method is new. The results show the following. First, 16APSK with MMSE equalization outperforms SOQPSK-TG with CMA equalization for the RHCP and LHCP channels. Second, 16APSK with MMSE equalization outperforms SOQPSK-TG with CMA equalization for the maximum likelihood channels at moderate to high signal-to-noise ratios. For lower signal-to-noise ratios, SOQPSK-TG shows the best performance. Third, 16APSK with MMSE equalization operating the maximum likelihood combined channel outperforms SOQPSK-TG with CMA equalization operating on the RHCP or LHCP channels.

INTRODUCTION

16APSK is a candidate modulation for improving spectral efficiency in aeronautical telemetry application, specifically when compared to SOQPSK-TG. To be accepted as a common modulation technique in aeronautical telemetry, the performance of 16APSK in real world scenarios such as frequency selective multipath fading is required.

In this paper we evaluate and compare the performance of 16APSK and SOQPSK-TG modulations, in the presence of polarization diversity and equalization in the receiver side. The constant modulus algorithm (CMA) is used to adaptively equalize SOQPSK-TG signal, and a minimum mean squared error (MMSE) equalizer is applied to 16APSK signal to take care of the channel impairments. For each signal two diversity combining techniques will be examined and simulated, the first one is combining the V and H polarizations in the receive antenna feed using a 90° hybrid

coupler and the second is maximum likelihood (ML) combiner. The first combining technique is the one currently used at most test ranges. The V and H polarizations combined using the 90° hybrid coupler are called circularly polarized signals. Most receive antenna produce two variants, RHCP and LHCP. The second combining technique is new and was developed for 16APSK in [1].

The simulation results show that for both modulations, ML combining outperforms the combining based on the 90° hybrid coupler. The computer simulation results also show that 16APSK modulation outperforms the SOQPSK-TG modulation in terms of the BER when we compare the RHCP and LHCP combined signals, and this is true for all the examined signal-to-noise ratios. However, the ML combined signal with SOQPSK-TG modulation outperforms ML combined signal with 16APSK for the lower values of signal-to-noise ratio.

SYSTEM MODEL

Complex valued baseband representations [2] will be used in the development. The transmitted signals, 16APSK and SOQPSK-TG, are described as follows:

- 16APSK is a signal of the form

$$s(t) = \sum_{\ell} a_{\ell} p(t - \ell T_s) \quad (1)$$

where a_{ℓ} is the ℓ -th transmitted symbol; T_s is the symbol time; and $p(t)$ is a unit energy square-root raised cosine (SRRC) pulse shape parameterized by the roll-off factor $0 \leq \alpha \leq 1$ [3]. The 16-APSK constellation is shown in Figure 1. The constellation is parameterized by the ratio of radii $\gamma = r_2/r_1$ and the phase angle ϕ .

- SOQPSK-TG is a constant phase modulation (CPM) of the form

$$s(t) = e^{j\phi(t; \mathbf{b})} \quad (2)$$

where $\phi(t; \mathbf{b})$ is the instantaneous phase that is a function of time and the bit sequence $\mathbf{b} = b(0), b(1), \dots$ and is defined as

$$\phi(t; \mathbf{b}) = 2\pi h \sum_k \alpha(k) q(t - kT_b) \quad (3)$$

where $h = 1/2$ is the modulation index; T_b is the bit time; $q(t)$ is the phase response usually described as the integral of a frequency pulse $f(t)$; and $\alpha(k)$ is the k -th modulating symbol given by

$$\alpha(k) = \frac{1}{2} (-1)^{k+1} a(k-1) [a(k) - a(k-2)] \quad (4)$$

where

$$a(k) = \begin{cases} -1 & b(k) = 0 \\ +1 & b(k) = 1. \end{cases} \quad (5)$$

(4) and (5) also show how the modulating symbols are related to the bit values. The frequency pulse spans 8 bit times and is elaborated in [4] (see also [5, 6]).

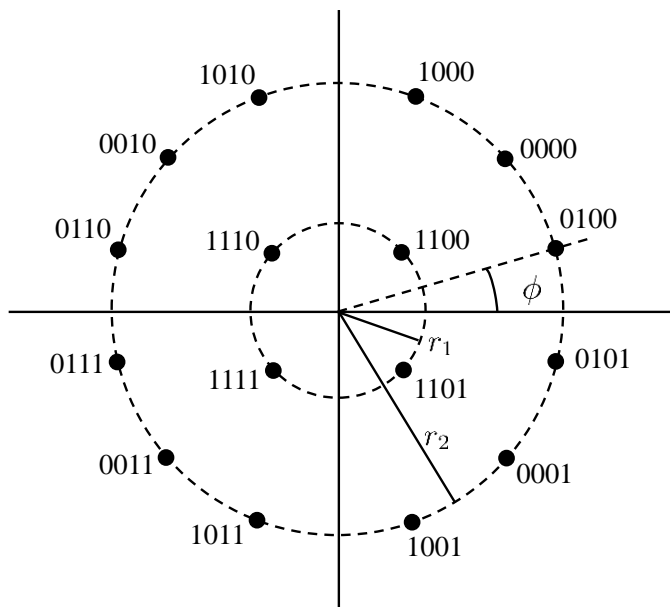


Figure 1: The 16-APSK constellation with the DVB-S2 bit-to-symbol mappings

The receiver captures the two polarization states of the received signal. The multipath channel is *different* in the two polarization states. This difference presents a form of diversity that can be exploited to improve the performance of the equalizers. The polarization properties of multipath scenario are discussed in the next Section. Applying diversity combining techniques, described later in this paper, on the corresponding channel impulse responses leads to a combined signal that is given by

$$r(t) = s(t) \star c(t) + z(t) \quad (6)$$

where $s(t)$ is the transmitted signal given by (1) or (2), \star is the continuous-time convolution operator, $c(t)$ is the combined channel, and $z(t)$ is a circularly-symmetric complex-valued wide-sense stationary normal random process representing the additive noise. The autocorrelation of $z(t)$ is a function of the combining techniques described in the below.

POLARIZATION-DEPENDENT MULTIPATH PROPAGATION

The multipath scenario shown in Figure 2 is used in this paper. Two coordinate systems are provided to be used, one is (x, y, z) Cartesian coordinate system, whose origin is shown in the figure, and the second one is (x', y', z') , whose origin is center of the parabolic reflector. The latter coordinate system is related to the former one by a translation along the x -axis and by a rotation over the y -axis by the antenna elevation angle, that is a function of the height of the transmitter antenna, height of the receiver antenna, and the ground distance (D) between the transmitter and receiver antennas.

Low elevation scenarios such as the one shown in Figure 2 can be modeled by a channel

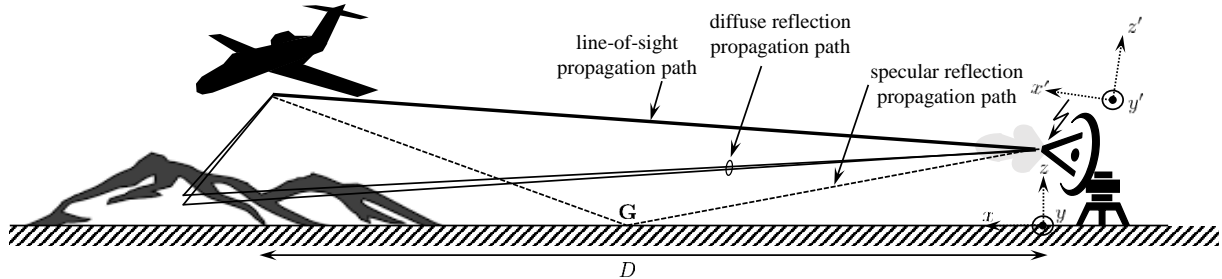


Figure 2: The geometry of multipath propagation for a land-based test range in the Western USA

comprising three propagation paths: a line-of-sight (LOS) path, a specular reflection that models a significant reflection from the ground in our scenario, and a diffuse scattering term that is basically a number of weaker reflections due to the rough surfaces such as mountain sides.

Polarization state information is used in multipath propagation for the LOS, and specular reflection as explained in [7]. The diffuse scattering term is modeled based on both measurements [8] and theory [9].

The transmitter is a vertically polarized antenna mounted on the bottom of the fuselage of an airborne test article, the receiver is a parabolic reflector with a resonant cavity at its focal point. The resonant cavity is equipped with a cross polarized dipole comprising vertically and horizontally polarized antenna elements in the directions of z' and y' respectively. Putting all the terms together channel impulse responses at the horizontally and vertically antenna feed outputs are as follows:

$$c_{y'}(t) = c_{y',0}\delta(t) + c_{y',1}\delta(t - \tau_1) + c_{y',2}\delta(t - \tau_2) \quad (7)$$

$$c_{z'}(t) = c_{z',0}\delta(t) + c_{z',1}\delta(t - \tau_1) + c_{z',2}\delta(t - \tau_2). \quad (8)$$

The received signals are also defined as

$$r_H(t) = c_{y'}(t) \star s(t) + z_H(t) \quad (9)$$

$$r_V(t) = c_{z'}(t) \star s(t) + z_V(t) \quad (10)$$

where $s(t)$ is given by (1) or (2), \star is the continuous-time convolution operator, and $z_H(t)$ is a circularly-symmetric complex-valued normal random process with zero mean and autocorrelation function [2]

$$E\{z_H(t + \tau)z_H^*(t)\} = 2N_0\delta(\tau), \quad (11)$$

and $z_V(t)$ is a complex-valued random process with identical statistics but is independent of $z_H(t)$.

THE ANALYSIS AND SIMULATION RESULTS OF POLARIZATION DIVERSITY COMBINING FOR 16APSK AND SOQPSK-TG SIGNALS

Our purpose here is the evaluation and comparison of the different combining techniques applied to 16APSK and SOQPSK in the multipath channel. The post-equalizer bit error rate is used as the figure of merit. The systems include 16APSK and SOQPSK-TG modulators, demodulators, corresponding detectors, and the two combiners will be elaborated in this section and the simulation results will be presented. The combiners are 90° hybrid coupler combiner and ML combiner.

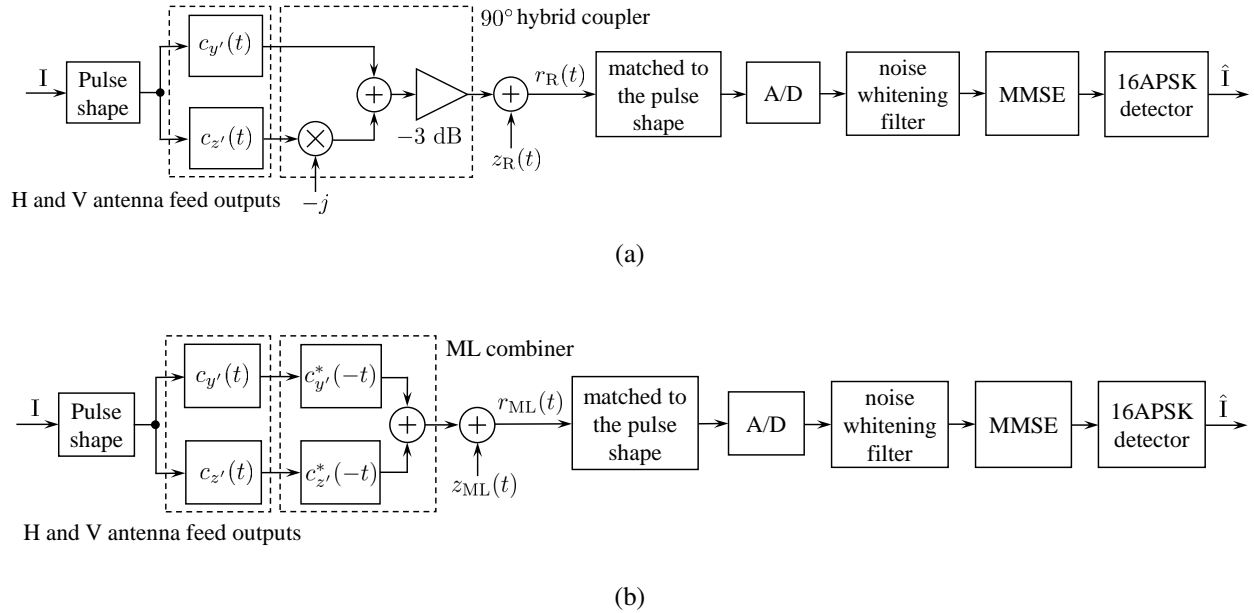


Figure 3: Block diagrams of the two combiners for 16APSK: (a) the combining performed by a 90° hybrid coupler to form an RHCP signal; (b) maximum likelihood combining.

- A 90° hybrid coupler combiner for 16APSK and SOQPSK signals are shown in Figures 3 (a) and 4 (a) respectively. The combined signal in 16APSK structure will be matched to the pulse shape filter after the noise addition, as shown in Figure 3 (a), however for SOQPSK signal, the output of the combiner will be applied to the CMA equalizer after the noise addition and analog-to-digital converter. Almost all of the receive antennas deployed at test ranges use a 90° hybrid coupler to construct the circularly (more accurately elliptically) polarized signals, designated RHCP and LHCP, from the linearly polarized (V and H) received signals. This structure is developed for 16APSK modulation scheme in [1], which based on it the development for SOQPSK-TG is straightforward.
- ML combiner in the structure of 16APSK and SOQPSK waveforms are shown in Figures 3 (b) and 4 (b). The combined signal in 16APSK structure will be matched to the pulse shape after the noise addition as shown in Figure 3 (b), however again for SOQPSK signal, the output of the combiner will be applied to the CMA equalizer after the noise addition and analog-to-digital converter. This difference comes from different signal modeling of linear and nonlinear waveforms [2]. ML combiner is developed for 16APSK and SOQPSK modulation schemes in [1] and [10] respectively.

The computer simulations are developed for the scenario shown in Figure 2, where the location of the transmitter and receiver antennas, the specular reflection point G , the refractive index at the specular reflection point, the ground distance between the transmitter and receiver antennas D along with yaw, pitch, and roll rotation angles for the test article are indicated in Table 1. The

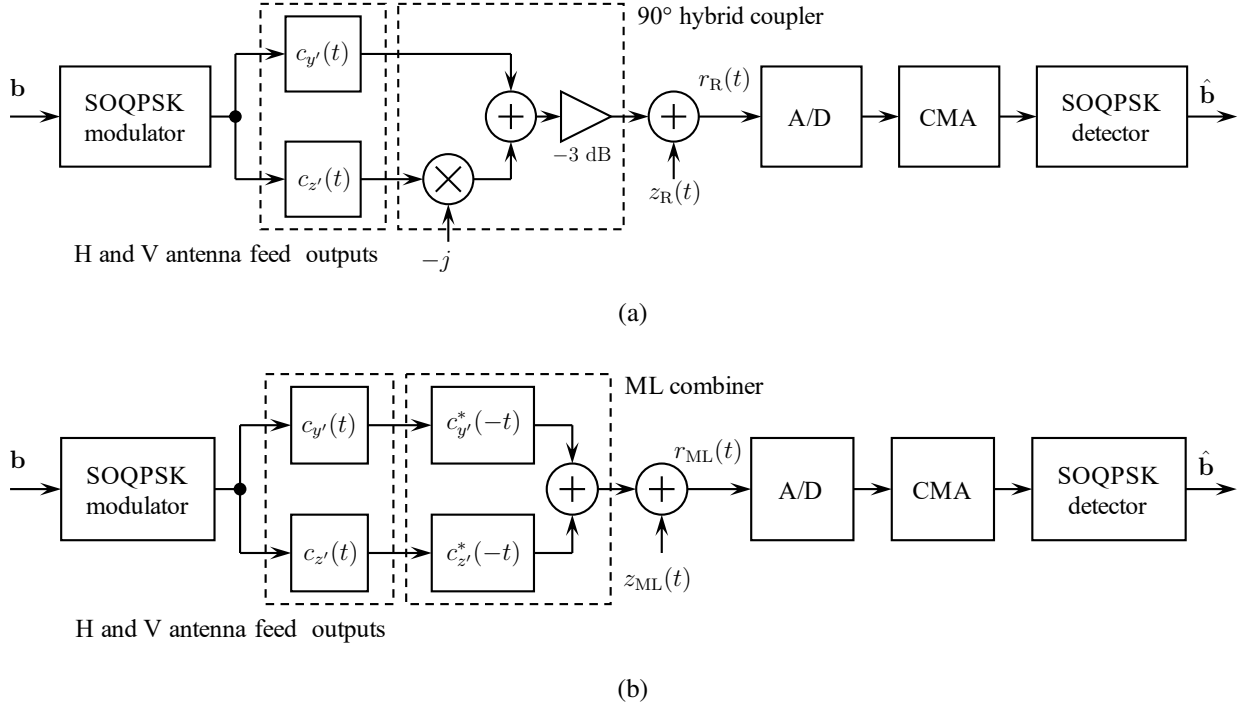


Figure 4: Block diagrams of the two combiners for SOQPSK-TG: (a) the combining performed by a 90° hybrid coupler to form an RHCP signal; (b) maximum likelihood combining.

channel coefficients and corresponding delays in (7) and (8) for such a scenario are:

$$\begin{aligned}
 c_{y',0} &= 0.2319 \\
 c_{y',1} &= -0.2533 + j0.0000 \\
 c_{y',2} &= -0.0621 - j0.0571 \\
 c_{z',0} &= 0.9543 \\
 c_{z',1} &= -0.9060 - j0.0000 \\
 c_{z',2} &= -0.0639 - j0.0256 \\
 \tau_1 &= 8.251 \text{ ns} \\
 \tau_2 &= 155 \text{ ns}.
 \end{aligned} \tag{12}$$

Note that $c_{y',2}$ and $c_{z',2}$ are calculated based on the realization of the random variable that describes the vertically polarized component [11], [12]. The channel transfer functions (CTF) of $c_{y'}(t)$ and $c_{z'}(t)$ are shown in Figure 5, then the corresponding CTF for RHCP and LHCP channels, and also for ML channel are shown in Figures 6 and 7 respectively. The power spectral density of 16APSK, and the power spectral density of SOQPSK-TG also are shown in Figures 5, 6, and 7.

BER curves are simulated for 16APSK and SOQPSK-TG modulations over all the channels shown in Figures 6 and 7. The computer simulations parameters setting for the system designs including 16APSK and SOQPSK waveforms are summarized in Tables 2 and 3 respectively. Note that the 16APSK constellation parameters shown in Table 2 are those that minimize the peak E_b/N_0 required to achieve a performance goal [13].

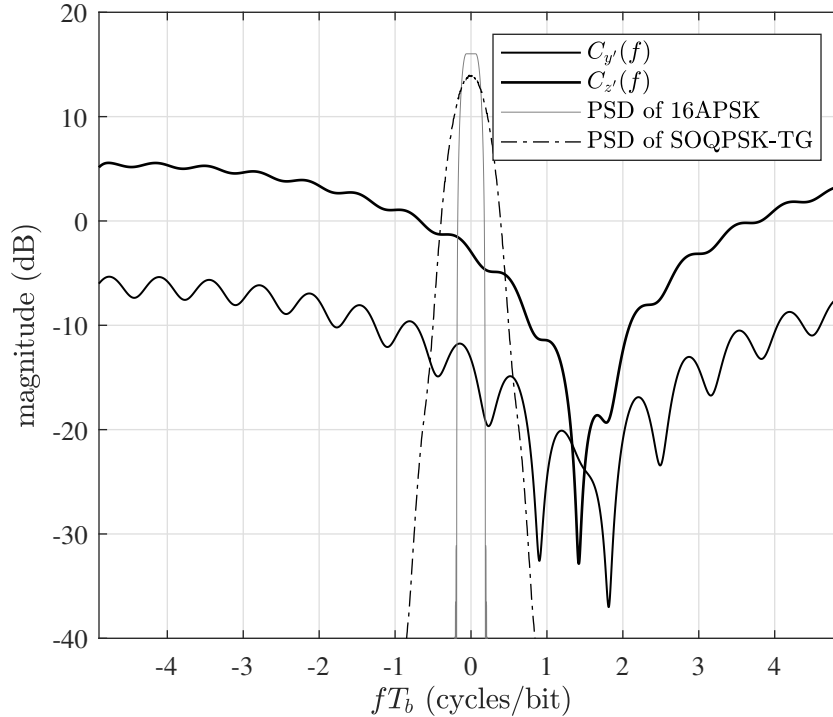


Figure 5: The transfer function of channels $c_{y'}(t)$ and $c_{z'}(t)$

The simulated BER performance is shown in Figure 8. The results show that for both waveforms the ML combiner outperforms 90° hybrid coupler as the combiner to produce either RHCP or LHCP signals. The results also show that 16APSK has a lower BER compare to SOQPSK-TG waveform that we simulated when compare the performance of RHCP or LHCP channels in terms of BER and this is true for all the LOS E_b/N_0 values, however ML combined channel with SOQPSK-TG waveform outperforms ML combiner channel with 16APSK waveform for the lower values of LOS E_b/N_0 , but for the higher values of LOS E_b/N_0 again 16APSK waveform is a winner.

CONCLUSIONS

We compared the post-equalizer performance of the 16APSK to SOQPSK-TG in a frequency-selective multipath environment. Two different polarization diversity combining techniques were examined: the 90° hybrid coupler that produces the RCHP and LHCP outputs commonly used at test ranges, and the ML combiner. The computer simulation results show that for both modulations ML combining outperforms 90° hybrid coupler combiner. The results lead to the following conclusions. First, 16APSK with MMSE equalization outperforms SOQPSK-TG with CMA equalization for the RHCP and LHCP channels. Second, 16APSK with MMSE equalization outperforms SOQPSK-TG with CMA equalization for the maximum likelihood channels at moderate to high signal-to-noise ratios. For lower signal-to-noise ratios, SOQPSK-TG shows the best performance.

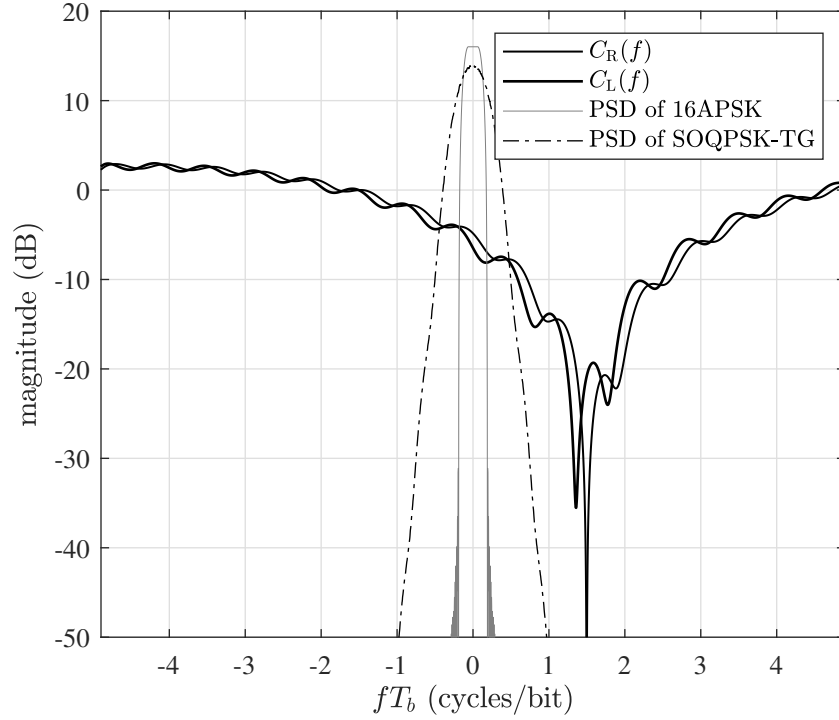


Figure 6: The transfer function of channels $c_R(t)$ and $c_L(t)$ shown in Figure 3 (a) and 4 (a)

Table 1: Geometry parameters corresponding to the scenario shown in Figure 2

Quantity	Value
T	(82139, -12521, 823) m
R	(0, 0, 125) m
G	(10831, 1651, 0) m
D	83,088 m
Refractive index at specular reflection	$1.7321 - j0.0007$
pitch	15°
yaw	5°
roll	10°

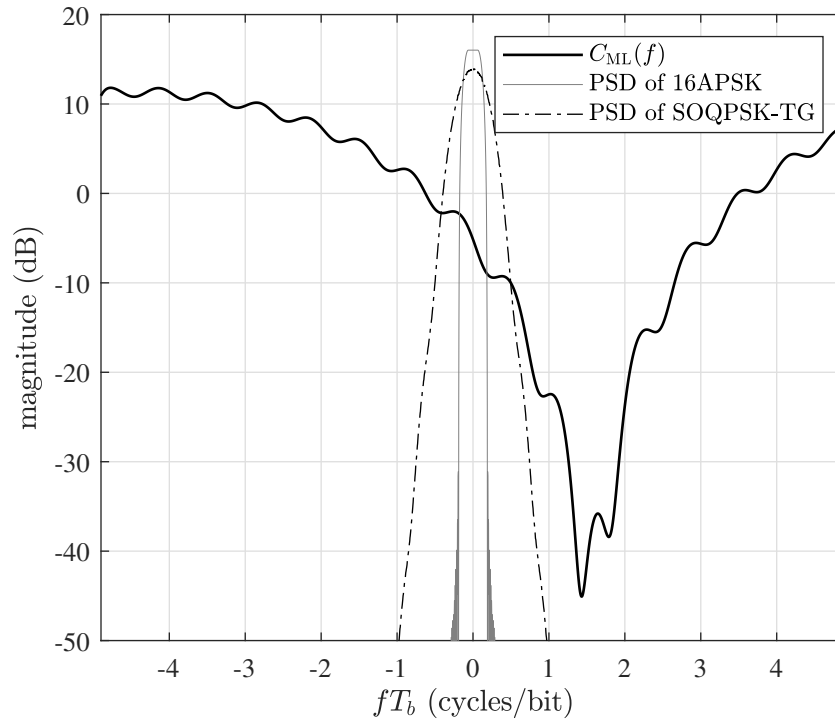


Figure 7: The transfer function of channel $c_{ML}(t)$ shown in Figures 3 (b) and 4 (b).

Table 2: The parameters used for the BER simulations of 16APSK.

Parameter	Value
Bit rate	10 Mbits/s
Carrier frequency	$f_c = 1485$ MHz (L Band)
Equalizer and detector sample rate	$N = 1$ samples/symbol
MMSE equalizer length	31 samples
Pulse shape	SRRC with roll-off factor 50%
γ	2.46
ϕ	$\pi/12$

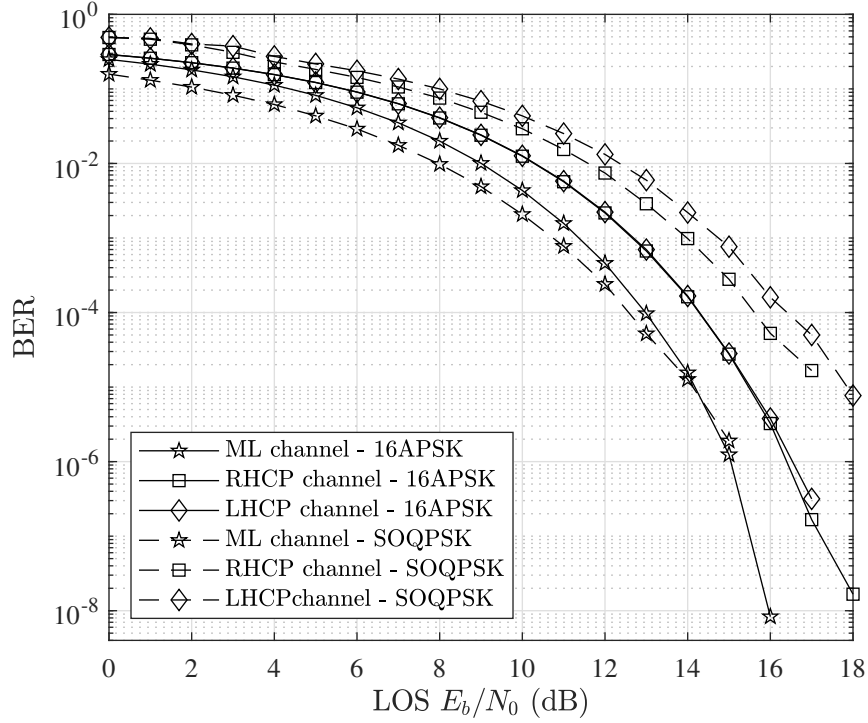


Figure 8: Simulated post-equalizer BER results using two combining techniques in the structures shown in Figures 3 and 4.

Table 3: The parameters used for the BER simulations of SOQPSK.

Parameter	Value
Bit rate	10 Mbits/s
Carrier frequency	$f_c = 1485$ MHz (L Band)
Equalizer and detector sample rate	$N = 2$ samples/symbol
CMA equalizer length	31 samples
CMA step size	10^{-5}
Carrier phase PLL	$B_n T_s = 0.01, \zeta = 1$
Timing PLL	$B_n T_s = 0.01, \zeta = 1$

Third, 16APSK with MMSE equalization operating the maximum likelihood combined channel outperforms SOQPSK-TG with CMA equalization operating on the RHCP or LHCP channels.

ACKNOWLEDGEMENTS

The funding for this project is managed by the Test Resource Management Center (TRMC) and funded through the Spectrum Access R&D Program under Contract No. W15QKN-15-9-1004.

REFERENCES

- [1] F. Arabian, "Polarization diversity and equalization of frequency selective channels in telemetry environment for 16APSK," 2019.
- [2] J. Proakis and M. Salehi, *Digital Communications*. New York: McGraw-Hill, 5th ed., 2007.
- [3] M. Rice, *Digital Communications: A Discrete-Time Approach*. amazon.com: Kindle Digital Publishing, 2018. ISBN-10: 1790588561. ISBN-13: 978-1790588565.
- [4] RRC, "Telemetry standards, IRIG-106," tech. rep., Telemetry standards, 2020. Available at https://www.wsmr.army.mil/RCCsite/Documents/106-20_Telemetry_Standards/106-20_Telemetry_Standards.pdf.
- [5] E. Perrins and M. Rice, "Reduced-complexity approach to iterative detection of coded SO-QPSK," *IEEE Transactions on Communications*, vol. 55, pp. 1354–1362, July 2007.
- [6] T. Nelson, E. Perrins, and M. Rice, "Near optimal common detection techniques for shaped offset QPSK and Feher's QPSK," *IEEE Transactions on Communications*, vol. 56, pp. 724–735, May 2008.
- [7] F. Arabian, G. Nordin, and M. Rice, "On the Ungerboeck and Forney observation models for spatial combining and their application to 5G millimeter-wave bands," *IEEE Access*, vol. 9, pp. 22214–22231, 9 February 2021.
- [8] M. Rice, A. Davis, and C. Bettweiser, "Wideband channel model for aeronautical telemetry," *IEEE Transactions on Aerospace and Electronic Systems*, vol. 40, no. 1, pp. 57–69, 2004.
- [9] P. Bello, "Aeronautical channel characterization," *IEEE Transactions on Communications*, vol. 21, no. 5, pp. 548–563, 1973.
- [10] F. Arabian and M. Rice, "Polarization combining and equalization for aeronautical mobile telemetry," in *MILCOM 2021 - 2021 IEEE Military Communications Conference (MILCOM)*, 2021 (forthcoming).
- [11] E. M. Vitucci, F. Mani, V. Degli-Esposti, and C. Oestges, "Study of a polarimetric model for diffuse scattering in urban environment," in *2012 6th European Conference on Antennas and Propagation (EUCAP)*, pp. 39–43, 2012.

- [12] Y. Yang, K.-S. Chen, X. Yang, Z.-L. Li, and J. Zeng, “Depolarized scattering of rough surface with dielectric inhomogeneity and spatial anisotropy,” *IEEE Transactions on Geoscience and Remote Sensing*, vol. 59, no. 1, pp. 47–59, 2021.
- [13] F. Arabian, W. Harrison, C. Josephson, E. Perrins, and M. Rice, “On peak-to-average power ratio optimization for coded APSK,” in *Proceedings of the IEEE International Symposium on Wireless Communication Systems*, (Lisbon, Portugal), 28–31 August 2018.